Magnetospheric electron densities inferred from upper-hybrid band emissions

R. F. Benson,[1] P. A. Webb,[2] J. L. Green,[1] L. Garcia,[3] and B. W. Reinisch[4]

Received 25 June 2004; revised 13 September 2004; accepted 21 September 2004; published 20 October 2004.

[1] The magnetospheric electron density N_e can often be obtained to within a few percent from passive radio-wave dynamic spectra when the electron plasma frequency f_{pe} ($\propto N_e^{1/2}$) is greater than the electron cyclotron frequency f_{ce}. This conclusion is based on interleaved active and passive observations from the Radio Plasma Imager (RPI) on the IMAGE satellite in the vicinity of the plasmapause. The N_e determinations are based on the frequency limits of an intense narrowband emission identified as the upper-hybrid band. The lower limit is identified with f_{pe} and the upper limit with the upper-hybrid frequency $f_{uh} = (f_{pe}^2 + f_{ce}^2)^{1/2}$. These frequency limits and the large amplitude of the emission, typically 20 dB or more above background, suggest strong Z-mode waves, rather than quasi-thermal fluctuations, as the emission source. *INDEX TERMS:* 2772 Magnetospheric Physics: Plasma waves and instabilities; 6984 Radio Science: Waves in plasma; 6939 Radio Science: Magnetospheric physics. **Citation:** Benson, R. F., P. A. Webb, J. L. Green, L. Garcia, and B. W. Reinisch (2004), Magnetospheric electron densities inferred from upper-hybrid band emissions, *Geophys. Res. Lett.*, *31*, L20803, doi:10.1029/2004GL020847.

1. Introduction

[2] Enhanced ionospheric and magnetospheric emissions are commonly observed by rocket- and satellite-borne radio receivers in the frequency range between the electron plasma frequency f_{pe} and the upper-hybrid frequency $f_{uh} = (f_{pe}^2 + f_{ce}^2)^{1/2}$ where f_{ce} is the electron cyclotron frequency. They correspond to the slow branch of the extraordinary mode, i.e., the Z mode, and are often referred to as upper-hybrid band emissions. Since the first observations, they have been attributed to non-thermal processes due to their large signal strength (typically 20 dB or more above background). Cherenkov radiation from energetic charged particles is considered the likely source mechanism because of the large refractive index (and hence low wave phase velocities) in this frequency domain [*Walsh et al.*, 1964]. Their importance in determining the magnetospheric electron density N_e {since $(f_{pe}\,(\mathrm{kHz}))^2 \approx 80.6\, N_e\, (\mathrm{cm}^{-3})$} was first convincingly demonstrated by *Bauer and Stone* [1968]. Determining the magnetospheric N_e from intense upper-hybrid band emissions is still considered to be the most reliable passive technique [*Denton et al.*, 2002]. An uncertainty is introduced, however, if this determination is based strictly on the observed emission-frequency maximum amplitude f_{mx} since it has been observed that while f_{mx} agrees with f_{pe} or f_{ce} to within about 5% for large f_{pe}/f_{ce} ($\approx$4), it can differ from f_{pe} or f_{ce} by as much as 20% for smaller f_{pe}/f_{ce} (<3) [*Benson et al.*, 2002]. In addition, evidence has been presented that inside the plasmasphere, where $f_{pe} \gg f_{ce}$, this emission line corresponds to quasi-thermal fluctuations near f_{pe} [*Lund et al.*, 1994]. The theory and observational evidence for such fluctuations near f_{pe} when $f_{pe} \gg f_{ce}$ has been presented in numerous publications but the treatment in a magnetized plasma is more difficult and in this case the observed emission line has been attributed to quasi-thermal fluctuations near f_{uh} [e.g., see *Meyer-Vernet et al.*, 1998, and references therein]. Here this emission line is investigated for the magnetospheric conditions when f_{pe} is comparable to, and greater than, f_{ce}. Specifically, we investigate the relationship of f_{mx}, and the lower and upper frequency limits f_{lo} and f_{up}, respectively, of the upper-hybrid band emission enhancement to f_{pe} and f_{uh}. Data from the Radio Plasma Imager (RPI) [*Reinisch et al.*, 2001] on the Imager for Magnetopause-to-Aurora Global Exploration (IMAGE) satellite [*Burch*, 2003] are used to compare f_{pe} and f_{uh}, determined to within a few percent from active (sounder) measurements, with f_{lo}, f_{mx} and f_{up}, also determined to within a few percent, from nearly simultaneous passive receiver measurements. The AUREOL/ARCADE-3 active (mutual impedance)/passive comparisons of *Beghin et al.* [1989], between f_{mx} and f_{pe} and f_{uh} and relating f_{pe} and f_{uh} to f_{lo} and f_{up}, respectively, claimed similar accuracy but were limited to low altitudes (400–2000 km). (IMAGE is in a highly elliptical polar orbit extending to 8-R_E radial distance.) The Cassini active (sounder)/passive comparisons of *Kurth et al.* [2001] achieved higher altitudes but was limited by a single pass through the magnetosphere, only a brief (5 min) period of active operation and an estimated 5% accuracy Langmuir-probe f_{pe} determination. The goal here is to make numerous active/passive comparisons in the region near and just beyond the plasmapause, so as to cover a range of f_{pe}/f_{ce} values, in order to determine if (1) f_{lo} and f_{up} can be identified with f_{pe} and f_{uh}, respectively or (2) f_{mx} can be identified with f_{uh}. As per the above discussion, the former conclusion would support a non-thermal Z-mode emission process whereas the latter would support quasi-thermal fluctuations as the source mechanism. A resolution of this question would allow numerous existing passive plasma-wave data sets, and passive plasma-wave data from future missions,

[1]NASA/Goddard Space Flight Center, Greenbelt, Maryland, USA.
[2]Nomad Research, Arnold, Maryland, USA.
[3]QSS Group, Inc., Greenbelt, Maryland, USA.
[4]Center for Atmospheric Research, Department of Environmental, Earth, and Atmospheric Sciences, University of Massachusetts, Lowell, Massachusetts, USA.

0094-8276/04/2004GL020847$05.00

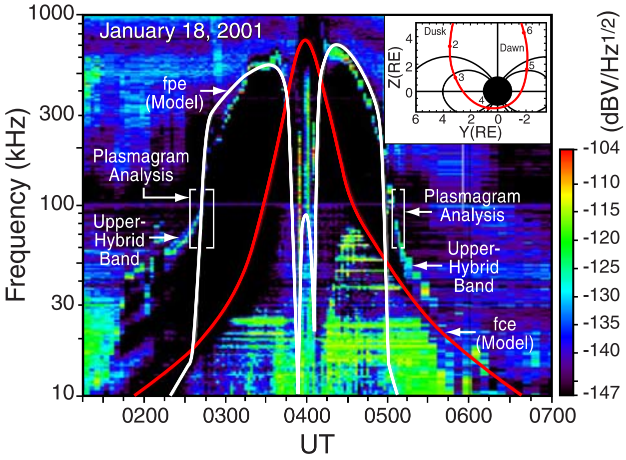

Figure 1. IMAGE/RPI passive dynamic spectrum with insert showing the IMAGE orbit in red and orbit-plane projections of the L = 4 and 8 dipole magnetic-field lines in black.

to be analyzed with confidence to make reliable N_e determinations.

2. Observations

[3] The RPI alternates between active and passive measurements. It employs three mutually orthogonal dipole antennas. Presently, the estimated tip-to-tip lengths of the spin-plane X and Y antennas are 370 m and 470 m, respectively, while the spin-axis Z dipole is 20 m. The RPI active measurements are displayed in the form of plasmagrams. They display the received signals recorded on one of the dipoles, following pulsed transmissions from the X dipole, and are used to determine f_{ce} (to within ~0.1%) and f_{pe} (to within ~1%) from the stimulated plasma resonances and the Z- & X-mode wave cutoffs [*Benson et al.*, 2003]. The plasmagrams presented here are based on X-dipole reception. The RPI passive measurements are displayed in the form of dynamic spectra (composed of spectral line scans typically separated by 2 minutes). They display signals from space-plasma emission processes and are used to determine (to within ~1%) f_{lo}, f_{up}, and f_{mx} of the upper-hybrid band emission enhancement. The dynamic spectra presented here are based on the combined signals from the X & Y dipoles so as to smooth out antenna spin-modulation effects. This study is based on a comparison of the interleaved passive and active RPI data. The sounder-derived f_{pe}, f_{ce} and f_{uh} values are linearly interpolated between successive active plasmagrams to the time of the upper-hybrid band emission enhancement, on an intervening passive dynamic spectral line scan, and compared with f_{lo}, f_{up}, and f_{mx}.

[4] The data are from three plasmapause crossings on 18 January 2001, when the IMAGE orbit was nearly normal to the plasmapause boundary, and one pass from 25 March 2003 when the IMAGE orbit was nearly tangent to the plasmapause boundary. The RPI dynamic spectrum in Figure 1 shows two of the plasmapause crossings.

[5] Figure 2 shows plasmagrams from two time intervals investigated. The most prominent sounder-stimulated plasma resonances and wave cutoffs, including the Dn and Qn resonances observed between the nf_{ce} harmonics, are identified. Such a rich spectrum offers redundancy that adds confidence in the determination of f_{pe} which, as illustrated in Figure 2b, does not always correspond to the strongest resonance [*Benson et al.*, 2003].

[6] The f_{ce}, f_{pe} and f_{uh} determinations from plasmagrams, such as those shown in Figure 2, were used to estimate the values for these parameters at the appropriate times on the intervening dynamic spectral line scans. Such scan lines, when combined, make up passive dynamic spectra of the type shown in Figure 1. The relative times between the active plasmagrams and the passive dynamic spectral line scans are shown in Figure 3; f_{ce}, f_{pe} and f_{uh} interpolations onto two consecutive dynamic spectral line scans from one of the cases investigated are shown in Figure 4.

[7] The main uncertainty in this comparison is the linear interpolation of the f_{pe} values with respect to time during the few minutes of orbital motion separating active soundings. The offset observed in the left panels of Figure 4 between the vertical lines, marking the interpolated f_{pe} and f_{uh} values, and the open circles and squares marking f_{lo} and f_{up} is attributed to this uncertainty. In the next dynamic spectrum, shown in the right panels of Figure 4, there was

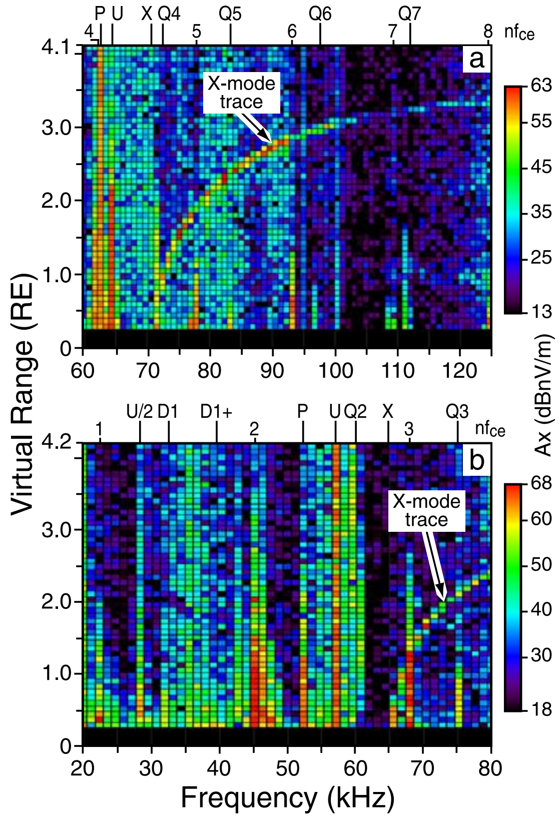

Figure 2. (a) Plasmagram with 0.9 kHz frequency steps from 18 Jan 2001 0237:16 UT (f_{pe}/f_{ce} = 62.6/15.6 = 4.0 based on plasma resonances at f_{pe}, f_{uh}, nf_{ce} and the X-mode wave cutoff designated by p, u, n and x, respectively). (b) Plasmagram with 1.2 kHz frequency steps from 25 March 2003 0047:09 UT (f_{pe}/f_{ce} = 52.5/22.7 = 2.3 determined as in (a) above). The Qn and Dn identifications correspond to the calculated positions [see *Benson et al.*, 2003].

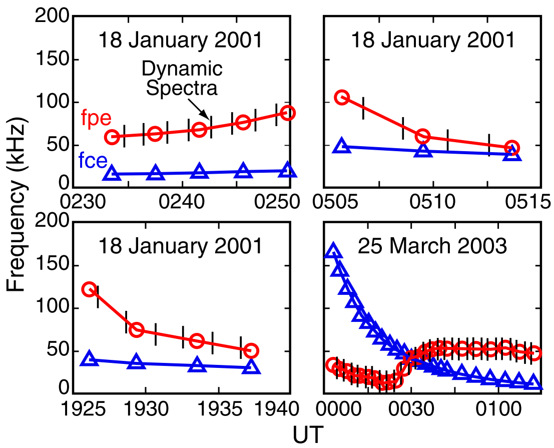

Figure 3. Values for f_{ce} (open blue triangles) and f_{pe} (open red circles) from the plasmagrams, and the times (vertical black line segments) of the intervening dynamic spectral line scans, for the four time intervals investigated. Straight lines connect the f_{ce} and f_{pe} values.

exact agreement between the interpolated f_{pe} and f_{uh} values and the steep edges of the signal enhancement. In addition to comparing individual cases as in Figure 4, a combined comparison was made to the dynamic spectra of Figure 3 with $f_{pe}/f_{ce} > 1$. This combined comparison tends to average out the interpolation uncertainties. The results, where all frequencies are normalized by f_{ce}, are presented in Figure 5.

[8] The statistical results of Figures 5a and 5b indicate that while the gradients for the comparisons between f_{mx} and f_{pe} and f_{uh} are equal to or near unity, the intercepts do not equal zero. Unity gradients and zero intercepts are achieved, however, in the results presented in Figures 5c and 5d where f_{lo} and f_{up} are compared to f_{pe} and f_{uh},

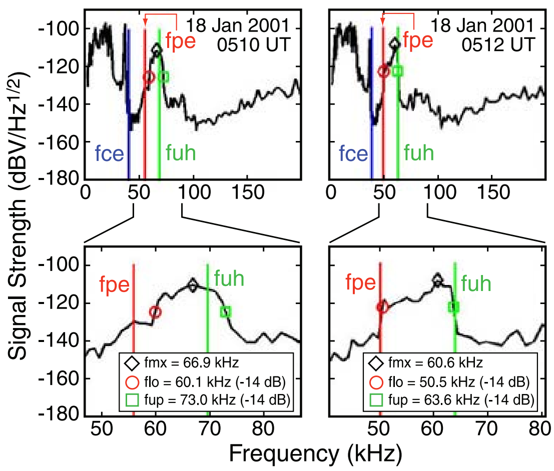

Figure 4. Two consecutive passive dynamic spectral line scans with superimposed interpolated frequencies from active plasmagrams. The lower panel enlargements clearly show the relationship between the interpolated f_{pe} and f_{uh} values (red and green vertical lines, respectively) and the observed f_{lo} (open red circles), f_{mx} (open black diamonds) and f_{up} (open green squares). (f_{pe}/f_{ce} (interpolated) = 56.2/41.4 = 1.4 and 50.2/39.7 = 1.3 in the left and right panels, respectively.)

respectively. Thus these statistical results support the impression given in the lower right panel of Figure 4, i.e., that f_{pe} corresponds to f_{lo} and f_{uh} corresponds to f_{up}. The Figure 5 results are dependent on the f_{lo} and f_{up} edge definitions. Too small a signal drop from the f_{mx} value leads to results more subject to the background noise level since the f_{mx} level is often only a few dB above the general upper-hybrid band enhancement of about 20 dB or more (see the bottom panels of Figure 4). Too large a signal drop leads to results more subject to the influence of adjacent resonances and the background noise level. The 14 dB value used in Figures 4 and 5 was selected because it gave gradient and intercept values of 1.00 and 0.00 (within the linear-regression uncertainties), respectively, in Figures 5c and 5d while maintaining high linear-regression coefficients ($\geq$0.984 for signal drop $\leq$14 dB). Approximately half of the errors indicated in Figure 5 are due to the one value near $f_{pe}/f_{ce} = 3$ and $f_{uh}/f_{ce} = 3$, well below the straight-line fit, in the left and right panels of Figure 5, respectively (the corresponding intercept values would change slightly by removing this point, i.e., they would become 0.22, -0.19, 0.01 and -0.01 in panels a, b, c and d, respectively). It corresponds to the 1926 UT dynamic spectral line scan in the lower left panel of Figure 3. Here the true negative f_{pe} gradient, just beyond 1925 UT, was apparently much steeper than indicated by the linear interpolation.

[9] In addition to the active/passive comparisons shown in Figures 4 and 5, a comparison was made that did not introduce interpolation assumptions. It is presented in Figure 6. Here plasmagram-determined f_{ce}, f_{pe} and f_{uh} values from active sounding were superimposed on the passive RPI dynamic spectrum corresponding to the same time interval. The upper-hybrid band is relatively broad

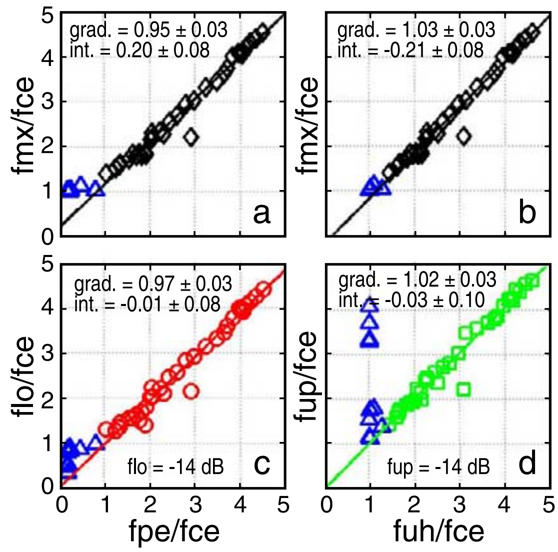

Figure 5. Combined normalized comparisons of the 35 $f_{pe}/f_{ce} > 1$ dynamic spectra of Figure 3. (a and b) f_{mx} compared to the interpolated f_{pe} and f_{uh}, (c) f_{lo} compared to the interpolated f_{pe}, and (d) f_{up} compared to the interpolated f_{uh}. The gradient and ordinate-axis intercept in each case were based on fitting only the $f_{pe}/f_{ce} > 1$ data to a straight line. The blue open triangles, corresponding to $f_{pe}/f_{ce} < 1$, were not used in this fitting.

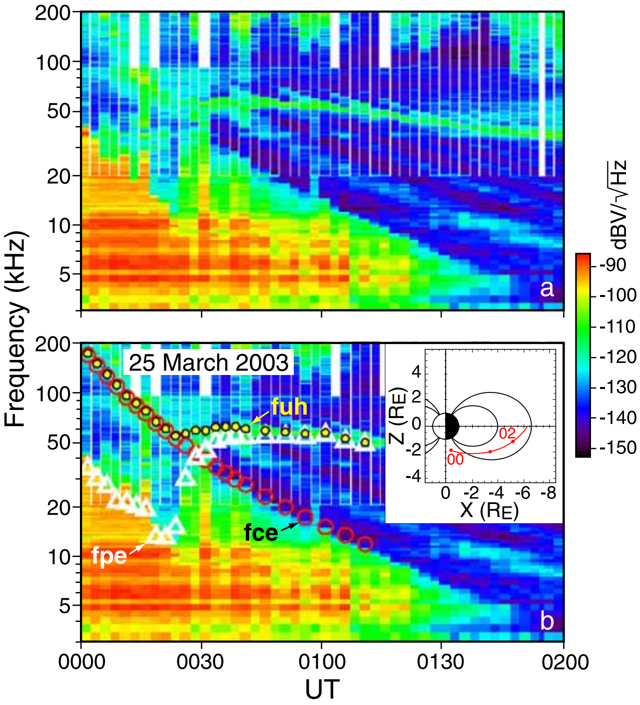

Figure 6. (a) Passive RPI dynamic spectrum. (b) Same as (a) except with superimposed f_{ce}, f_{pe} and f_{uh} values determined from active RPI plasmagrams.

(extending from ≈50 to 60 kHz) near 00:30 UT where $f_{pe} \approx f_{ce}$ and it narrows in bandwidth as time progresses. The scaled f_{pe} and f_{uh} frequencies in the region beyond about 00:30 UT, i.e., in the region where $f_{pe} > f_{ce}$, allow the boundaries of the upper-hybrid band to be identified and distinguished from the slanting finger-like higher-frequency emissions. These emissions are attributed to Q_n emissions, which are often observed between the nf_{ce} harmonics at frequencies greater than f_{uh} [see, e.g., *Benson et al.*, 2003], and they can hinder an accurate determination of f_{up}. When $f_{pe} < f_{ce}$ the determination of f_{lo} can be compromised by the lack of a well defined emission peak.

3. Discussion and Conclusions

[10] The IMAGE/RPI active/passive comparisons presented here indicate that the upper-frequency edge f_{up} of the upper-hybrid band enhancement (of typically 20 dB) on passive RPI magnetospheric dynamic spectra is equal to f_{uh}, and the lower-frequency edge f_{lo} is equal to f_{pe}, when $f_{pe} > f_{ce}$ to an accuracy of a few per cent in f_{pe}. These results, which emphasize the importance of the frequency extremes of the large emission enhancement rather than the frequency of the maximum, support the non-thermal Z mode rather than the quasi-thermal mechanism. They were confirmed over a range of f_{pe}/f_{ce} values from approximately 1 to 5. Here we do not investigate possible source mechanisms for the Z-mode waves (often attributed to Cherenkov emission [e.g., see *Walsh et al.*, 1964; *Kurth et al.*, 2001]). The identification of f_{up} can be compromised by the presence of Qn emissions. Contrary to the findings of *Kurth et al.* [2001], we always observed the maximum of the upper-hybrid band enhancement at f_{mx} to be of greater intensity than these higher-frequency emissions; these differences, however, may be due to the shorter antennas employed by Cassini. Figure 6 illustrates the benefit of having active soundings to confidently determine f_{pe} when $f_{pe} < f_{ce}$. The sounder-derived f_{pe} values (white triangles) follow the upper edge of an intense, presumably whistler mode, emission. They deviate from this upper edge, however, at a location that would be difficult to determine without the benefit of active sounding. Also, in this $f_{pe} < f_{ce}$ frequency domain, the upper-hybrid band enhancement, in this case between f_{ce} and f_{uh}, is often not very well defined. Under these conditions f_{uh} approaches f_{ce}, as illustrated in Figure 6, and f_{mx} is identified with this combined frequency as indicated by the open blue triangles in Figures 5a and 5b. The weakness of the upper-hybrid band enhancement is illustrated by the vertical spreads in the open blue triangles in Figures 5c and 5d corresponding to small f_{pe}/f_{ce} values. These spreads are caused by the great frequency separations from f_{mx} required to achieve 14-dB signal reductions. *Beghin et al.* [1989] never observed an enhancement when $f_{pe} < f_{ce}$; they attribute this finding to a lack of instability growth of Z-mode waves in the upper-hybrid band under these conditions. This frequency domain, as well as the domain of $f_{pe} \approx f_{ce}$, requires more investigation.

[11] Plasmagrams such as the ones shown in Figure 2 provide multiple determinations of f_{pe}. Passive magnetospheric dynamic spectra can also often offer more than one determination of f_{pe} in the frequency domain $f_{pe} > f_{ce}$ (a common magnetospheric condition). Since N_e is proportional to f_{pe}^2, it can be determined either directly from f_{pe} or from f_{uh} with knowledge of f_{ce} from either a magnetic-field model or a scientific magnetometer. Thus two N_e determinations will result from the detection of the lower and upper frequency limits of the upper-hybrid band. When f_{pe} increases to beyond about $4f_{ce}$, where f_{uh} exceeds f_{pe} by <3%, the $f_{up} - f_{lo}$ separation becomes comparable to the instrument frequency resolution so that only a single estimate of f_{pe} is possible, namely, by considering f_{up} ($\approx f_{lo} \approx f_{mx}$) = f_{uh} ($\approx f_{pe}$).

[12] **Acknowledgments.** This work received support from NSF ATM-0245664, and from subcontract 83822 from Southwest Research Institute to UML under NASA contract NAS5-96020. We are grateful to D. L. Carpenter for helpful comments.

References

Bauer, S. J., and R. G. Stone (1968), Satellite observations of radio noise in the magnetosphere, *Nature*, *218*, 1145–1147.

Beghin, C., J. L. Rauch, and J. M. Bosqued (1989), Electrostatic plasma waves and HF auroral hiss generated at low altitude, *J. Geophys. Res.*, *94*, 1359–1379.

Benson, R. F., P. A. Webb, J. L. Green, and B. W. Reinisch (2002), Relating magnetospheric passive dynamic spectral emission peaks to plasma and upper-hybrid frequencies determined from active RPI sounding on IMAGE, *Eos Trans. AGU*, *83*(19), Spring Meet. Suppl., Abstract SM21A-06.

Benson, R. F., V. A. Osherovich, J. Fainberg, and B. W. Reinisch (2003), Classification of IMAGE/RPI-stimulated plasma resonances for the accurate determination of magnetospheric electron-density and magnetic field values, *J. Geophys. Res.*, *108*(A5), 1207, doi:10.1029/2002JA009589.

Burch, J. L. (2003), The first two years of IMAGE, *Space Sci. Rev.*, *109*, 1–24.

Denton, R. E., J. Goldstein, and J. D. Menietti (2002), Field line dependence of magnetospheric electron density, *Geophys. Res. Lett.*, *29*(24), 2205, doi:10.1029/2002GL015963.

Kurth, W. S., et al. (2001), An overview of observations by the Cassini radio and plasma wave investigation at Earth, *J. Geophys. Res.*, *106*, 30,239–30,252.

Lund, E. J., J. LaBelle, and R. A. Treumann (1994), On quasi-thermal fluctuations near the plasma frequency in the outer plasmasphere: A case study, *J. Geophys. Res.*, *99*, 23,651–23,660.

Meyer-Vernet, N., S. Hoang, K. Issautier et al. (1998), Measuring plasma parameters with thermal noise spectroscopy, in *Measurement Techniques in Space Plasmas: Fields*, *Geophys. Monogr. Ser.*, vol. 103, edited by R. F. Pfaff, J. E. Borovsky, and D. T. Young, pp. 205–210, AGU, Washington, D. C.

Reinisch, B. W., et al. (2001), First results from the radio plasma imager on IMAGE, *Geophys. Res. Lett.*, *28*, 1167–1170.

Walsh, D., F. T. Haddock, and H. F. Schulte (1964), Cosmic radio intensities at 1.225 and 2.0 Mc measured up to an altitude of 1700 km, in *Space Research*, edited by P. Muller, pp. 935–959, North-Holland, New York.

R. F. Benson, L. Garcia, J. L. Green, and P. A. Webb, NASA/Goddard Space Flight Center, Greenbelt, MD 20771, USA. (robert.f.benson@nasa.gov)

B. W. Reinisch, Center for Atmospheric Research, Department of Environmental, Earth, and Atmospheric Sciences, University of Massachusetts, Lowell, MA 01854, USA.